Numerical Investigation of Residual Displacement of Rocking Self-Centering Columns Under Cyclic Loading

Yan Shi
Lanzhou University of Technology
zhengwu zhong (zzw0730@163.com)
Lanzhou University of Technology https://orcid.org/0000-0002-3662-4320
Zhichao Zhang
Lanzhou University of Technology
Jianping Han
Lanzhou University of Technology
Hu Cheng
Jiangnan University

Research Article

Keywords: Rocking self-centering column, Residual displacement, Cyclic loading, Factorial analysis

Posted Date: July 16th, 2021

DOI: https://doi.org/10.21203/rs.3.rs-706183/v1

Numerical investigation of residual displacement of rocking self-centering columns under cyclic loading

Yan Shi[a], Zhengwu Zhong[a,*1], Zhichao Zhang[a], Jianping Han[a], Hu Cheng[b,*]

[a] School of Civil Engineering, Lanzhou University of Technology, Lanzhou730050, China

[b] School of Environment and Civil Engineering, Jiangnan University, Wuxi214122, China

Corresponding author.

E-mail addresses: syky86@163.com(Y. Shi), zzw0730@163.com (Z. Zhong) , Zhangzhic0303@163.com (Z. Zhang), jphan1970@163.com(J. Han), hcheng@jiangnan.edu.cn(C. Hu).

Numerical investigation of residual displacement of rocking self-centering columns under cyclic loading

Yan Shi[a], Zhengwu Zhong[a,*], Zhichao Zhang[a], Jianping Han, Hu Cheng[b,*]

[a] School of Civil Engineering, Lanzhou University of Technology, Lanzhou730050, China

[b] School of Environment and Civil Engineering, Jiangnan University, Wuxi214122, China

Abstract

Well-designed rocking self-centering (RSC) columns are capable of achieving small residual displacement. However, few studies conducted the quantitative analysis for the residual displacement of RSC columns. The residual displacement is the product of the struggle between the self-centering (SC) capacity and the energy dissipation (ED) capacity. In this study, a SC factor and an ED parameter were defined to reflect the SC and ED capacity of the RSC column, respectively. The influence of eight common design parameters on the SC factor and the ED parameter was explored using factorial analysis. Parametric analysis was performed to investigate the tendency of the SC factor and the ED parameter with the increase of maximum drift. According to the results of the parametric analysis, the effect of the SC factor and the ED parameter on the distribution of the residual drift was researched statistically. A simplified formula was proposed to calculate the upper limit of the residual drift. What is more, a set of predictive regression formulas was established to estimate the actual residual drift, these regression formulas have an applicable condition that the ED parameter should be larger

than 0.75. When the ED parameter was less than 0.75, the residual drift is approximate to zero.

Keywords Rocking self-centering column • Residual displacement • Cyclic loading • Factorial analysis

1. Introduction

Past devastating earthquakes have demonstrated that the reinforced concrete (RC) bridge structures are highly vulnerable to earthquakes with extensive damage concentrated in plastic region of bridge pier (Han et al. 2009; Shi et al. 2020). It is likely to cause large residual displacement as a result of serious damage. The bridge structure with significant permanent displacement is hard to return back to the initial position, which causes tremendous difficulties to the post-earthquake recovery and huge economic losses (Kawashima et al. 1998). For example, about 100 RC bridge piers were eventually demolished due to a residual drift ratio of 1.75% after the 1995 Kobe earthquake in Japan (Kawashima et al. 1998). Therefore, the residual displacement is regarded as a main index to evaluate the earthquake resilience and the self-centering capacity of piers become an important design consideration (Uma et al. 2010; Palermo and Mashal. 2012).

Based on accelerated bridge construction philosophy, the rocking self-centering (RSC) column was proposed, and the post-tensioning has been considered to be an efficient way to drastically reduce the residual displacement (Marsh et al. 2011). To data, many experimental studies have been carried out to address the seismic behavior of RSC columns (Hewes and Priestley. 2002; Palermo et al. 2007; Ou et al. 2010; Bu et al.

2016; Elgawady and Sha'lan. 2011; Guo et al. 2015; Han et al. 2019; Tong et al. 2019; Cai et al. 2017; Roh and Reinhorn. 2010). Hewes and Priestley (2002) performed an early cyclic test of the RSC column, the result shown that the segments of the pier basically remained elastic and the residual drift was very small. However, the energy dissipation (ED) capacity was extremely weak due to the lack of ED elements. To enhance the ED capacity of RSC columns, various types of dissipaters were proposed and the ED bar is the commonest ED device among these dissipaters. The results of many cyclic tests shown that the hysteretic curve of the RSC column equipped with ED elements was much fuller, and the ED capacity was improved as expected (Palermo et al. 2007; Ou et al. 2010; Bu et al. 2016; Elgawady and Sha'lan. 2011; Guo et al. 2015; Han et al. 2019). Meanwhile, the added ED elements reduced the SC capacity of RSC columns, leading to the problem of residual displacement could not be ignored if too many dissipaters were used. Some researchers tried to use high performance materials (e.g. shape memory alloy, fiber-reinforced polymer composite bar) to achieve a balance between SC and ED capacity (Tong et al. 2019; Cai et al. 2017; Roh and Reinhorn. 2010). It can be concluded that there is a trade-off between the SC and ED capacity, the residual displacement is the product of their mutual struggle.

The harm of residual displacement has been realized gradually, and residual displacement has been regarded as an important consideration in seismic design. According to earthquake damage investigation results, the Japan Road Association code first proposed a reparability limit of 1% for RC columns (Japan Road Association, 2002). Some researches focusing on the residual displacement of RC columns have

been conducted, aiming to explore the influence factors and achieve the estimation of residual displacement under earthquakes. It can be concluded that the residual drift is determined by structural properties and characteristics of earthquake load both (Liossatou and Fardis. 2016; Cheng et al. 2016; Liossatou and Fardis. 2015; Ji et al. 2018; Amiri and Bojorquez. 2019; Zhan and Jian. 2018; Quinde et al. 2019). However, few studies related to the residual displacement estimation of RSC columns have been reported. Li et al. (2020) selected residual drift as a performance index to conduct seismic vulnerability analysis and losses assessment of an RSC bridge system. Ou et al. (2007) developed a three-dimensional model of the RSC column equipped with internal ED bars, the results of cyclic loading analyses suggested an optimum ED bar ratio of 0.5% around. Cai et al. (2019) performed cyclic analyses to investigate the influence of post-tensioning force, gravity load, ED bar ratio and aspect ratio on the residual drift of RSC columns. Liu et al (2018) carried out parametric analyses on residual displacement under cyclic loading. Wang et al. (2019) proposed a simplified formula for UHPC bridge columns with unbonded post-tensioning tendons to calculate the upper limit of residual drift under cyclic loading. In conclusion, the residual drift of RSC columns under cyclic loading mainly depends on structural properties, quantitative analysis of residual drift is still limited in previous work.

The purpose of this study is exploring the distribution of residual drift of RSC columns under cyclic loading and achieving its prediction. Two governing parameters including a SC factor and an ED parameter were introduced to describe the SC capacity and ED capacity of piers. The contribution of eight common design parameters to the

84 SC factor and ED parameter was compared. Then the effect of the SC factor and ED
85 parameter on the residual drift was investigated, a set of predictive formulas for the
86 residual drift was obtained from regressive analyses and an application of it was given.

87 # 2. Simulation of RSC columns

88 ## 2.1 Simulation method

89 To capture the hysteretic behavior of the RSC columns, a numerical model is
90 established using OpenSees. Fig. 1 shows the schematic of the analytical model. The
91 displacement of the RSC columns is dominated by rigid rotation, the bending
92 deformation occurs before the column lifts up and its contribution is very small, so the
93 elastic beam-column elements can be used to model the column, this simplified
94 simulation strategy was also adopted in previous studies (Ahmdi and Kashani, 2020;
95 Marriott et al. 2009). A lumped mass is applied at the pier top to represent the gravity
96 load, and a horizontal constraint is set at the bottom to prevent the relative slide between
97 the column and the foundation. CorotTruss elements composed of
98 elastic-perfectly-plastic material are considered to model the force-displacement of the
99 unbonded post-tensioning (PT) tendons. The bottom nodes of the tendons are fixed, and
100 the top nodes are connected with the corresponding column node with rigid links. A
101 similar simulation method is adopted to model the unbonded segments of the energy
102 dissipation (ED) bars. Truss elements with Reinforcing Steel material are used to model
103 the ED bars, and the ultimate stress is set to 1.35 times as much as the yield stress f_y
104 (Priestley et al. 2007); the ratio of the tangent at initial strain hardening to the initial
105 elastic tangent can be set to 0.01-0.05 (Cai et al. 2019) (0.03 is selected in this study),

the ratio of strain corresponding to the initial strain hardening to the yield strain can be set to 3-5 (Cai et al. 2019) (3 is selected in this study), and the ultimate strain can be set to 0.1 (Kowalsky et al. 1995).

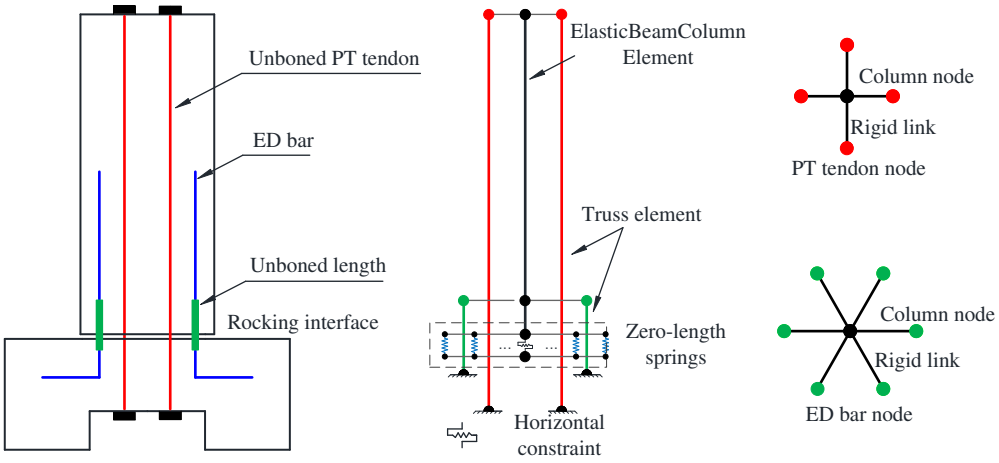

Fig. 1 Finite element model and cross-sections of existed test specimens

The total unbonded length of ED bars in numerical model, L_{ub}, consists of two parts. One is the designed unbonded length (L_0) which can prevent the early fracture of ED bars, the other is the equivalent unbonded length (L_{eu}) caused by the strain penetration. The L_{ub} can be expressed as:

$$L_{ub} = L_0 + L_{eu} \tag{1}$$

If L_{eu}=0, the value of L_{ub} is minimum, so the stress of ED bars is largest at the same lateral displacement. As a result, the strength of an RSC column will be overestimated. The value of L_{eu} is significant, but it is difficult to determine its value precisely because of the complexity of the strain penetration. For example, Mantawy et al. (2019) suggested to adopt an iterative method to determine the value of L_{ub}, the trial value of L_{ub} continued to increase until the correct bridge stiffness was calibrated.

Some formulas of L_{eu} can be found in the researches related to analytical pushover

123 method for RSC columns (Pampanin et al. 2001; Bu and Ou, 2013). According to the
124 monolithic beam analogy, the stress of ED bars can be expressed as follows (Pampanin
125 et al. 2001):

126 $$\varepsilon_{\mathrm{s}} = \frac{[(\Delta + 2/3 l_{\mathrm{sp}} \alpha \varepsilon_{\mathrm{y}})]}{(L_0 + 2l_{\mathrm{sp}})} \approx \frac{\Delta}{(L_0 + 2l_{\mathrm{sp}})} \quad (2)$$

127 where Δ is elongation of an ED bar, due to the opening of the joint; ε_{y} is yield strain
128 of ED bars; α is ratio of elastic strain and yield strain in reinforcement; l_{sp} is strain
129 penetration taken as $0.022 f_{\mathrm{y}} d_{\mathrm{b}}$, f_{y} and d_{b} are the yield stress and diameter of ED bars,
130 respectively. All units in MPa and mm. From Eq. (2), L_{eu} can be calculated as:

131 $$L_{\mathrm{eu}} = 2l_{\mathrm{sp}} = 2 \times 0.022 f_{\mathrm{y}} d_{\mathrm{b}} \quad (3)$$

132 In Bu's study, L_{eu} is calculated with Eq. (4) (Bu and Ou, 2013).

133 $$L_{\mathrm{eu}} = \begin{cases} 0 & , f_s > f_y \\ \dfrac{2.1 \times (f_s - f_y)}{(f_g)^{1.5}} d_{\mathrm{b}} & , f_s > f_y \end{cases} \quad (4)$$

134 where f_{s} is stress of ED bars; f_{g} is compression strength of grout.

135 By trial calculation, it can be found that the calculated results obtained from Eq. (3)
136 are much larger than the results of Eq. (4) generally. Therefore, Eq. (3) is used to
137 determine the maximum value of L_{ub}. Though the precise value of L_{ub} is hard to
138 determine, the range of L_{ub} can be estimated by Eq. (5), in the later analysis, the
139 influence of L_{ub} on residual displacement will be discussed.

140 $$\mathrm{Min}\, L_{\mathrm{ub}} = L_0 < L_{\mathrm{ub}} < L_0 + 2 \times 0.022 f_{\mathrm{y}} d_{\mathrm{b}} = \mathrm{Max}\, L_{\mathrm{ub}} \quad (5)$$

141 Several compression-only springs are used to model the opening and closing of the
142 bottom rocking interface. Generally, the simulation result will become stable gradually

as the number of springs increases. These springs are distributed in a uniform way, the distance between two adjacent springs is equal and all springs have the same axial stiffness. The axial stiffness, k, can be calculated as (Li et al, 2020):

$$k = \frac{2E_c A_g}{nH} \tag{6}$$

where $E_c = 4700\sqrt{f_c'}$ is the elastic modulus of the concrete, f_c' is the concrete compressive strength (Ahmdi and Kashani, 2020); A_g is the gross area of the column section; H is the column height; n is the number of zero-length springs.

2.2 Model validation

Table 1 Properties of selected specimen

Specimen	PT1	HBD2	HBD1	s-SCP(I-ED)
Geometry	350×350 mm	350×350 mm	350×350 mm	400×400 mm
Aspect ratio	4.57	4.57	4.57	3.78
Total axial load	200 kN	300k	200kN	533.05kN
Tendons	2×99 mm2	4×99 mm2	2×99 mm2	4Φ15.2
	100 kN each	75 kN each	100 kN each	313.05 kN total
Dissipation	None	4-HD20	4-D16	4-D20
		12.5 mm diameter fuse	reinforcing steel	reinforcing steel
		50 mm fuse length	L_0=50 mm	L_0=100 mm
		f_y=586 MPa	f_y=304 MPa	f_y=349 MPa

In order to validate the simulation method, 4 RSC bridge pier specimens are selected (Palermo et al. 2007; Guo et al, 2012), as reported in Table 1. PT1 has no dissipation elements, it can be used to confirm the effectiveness of the modeling methods for all components in addition to ED bars. HBD2 chooses the reinforcing steel with a fuse length as the dissipation element. HBD1 and s-SCP(I-ED) dissipate energy by the internal reinforcing steel, the corresponding unbonded length is 50 mm and 100 mm, respectively. More detailed information about these specimens can be found in

reference (Palermo et al. 2007; Guo et al, 2012).

As shown in Fig. 2, the numerical hysteretic curves are compared with the test results. For specimen PT1 as shown in Fig. 2(a), the simulated initial stiffness is slightly larger than the test result and the simulated strength was slightly lower. Besides, because the elastic beam-column element is adopted to model the column, the simulated hysteretic curve is unable to reflect the little energy dissipation during the cyclic loading. On the whole, the FE result matches well with the test result, which suggests that the simulation techniques except for ED bars are effective.

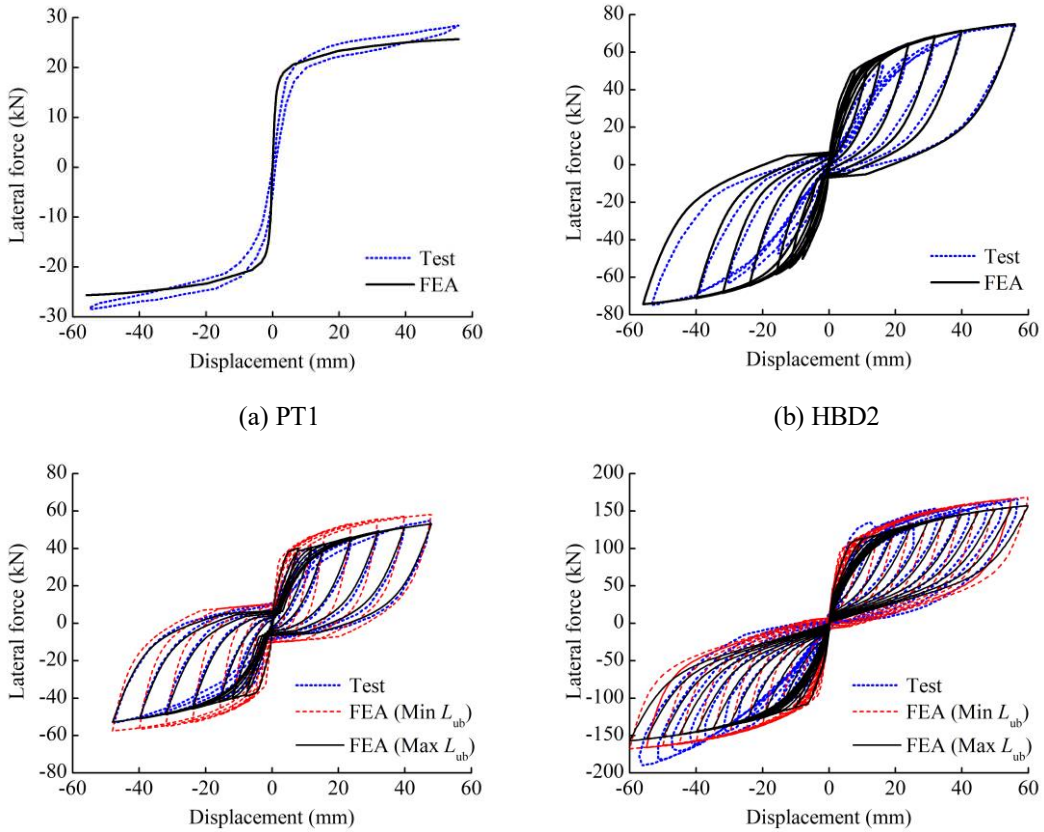

(a) PT1 (b) HBD2

(c) HBD1 (d) s-SCP(I-ED)

Fig. 2 Comparisons of the numerical hysteretic curve with the test results

Due to the reinforcing steel in specimen HBD2 has a fuse length of 50 mm, strain will be concentrated on the fuse segment, so L_{ub} is set to 50 mm. The hysteretic curve

based on FEA is plotted in Fig. 2(b). As for specimens HBD1 and s-SCP(I-ED), detailed comparisons between test and simulation results are presented in Fig. 2(c) and (d). The red and black curves represent the simulation results corresponding to the minimum L_{ub} and the maximum L_{ub}, respectively. The lateral strength of the red curves is slightly larger than the black curves, it is because a smaller L_{ub} will generate a larger strain under the same joint opening, larger strain leads to larger dissipation force. As a result, the lateral strength is improved. Meanwhile, the residual displacement per loop of the red curves is also larger than the black curves, detailed comparisons are plotted in Fig. 3. On the one hand, this phenomenon can be explained from the perspective of larger dissipation force which weakens the self-centering capacity of the piers. On the other hand, the increase of L_{ub} will decrease the slope of unloading path significantly and thus diminish the residual displacement as shown in Fig. 2(c) and (d). The latter reason is more important, because the improvement of dissipation force is very limited.

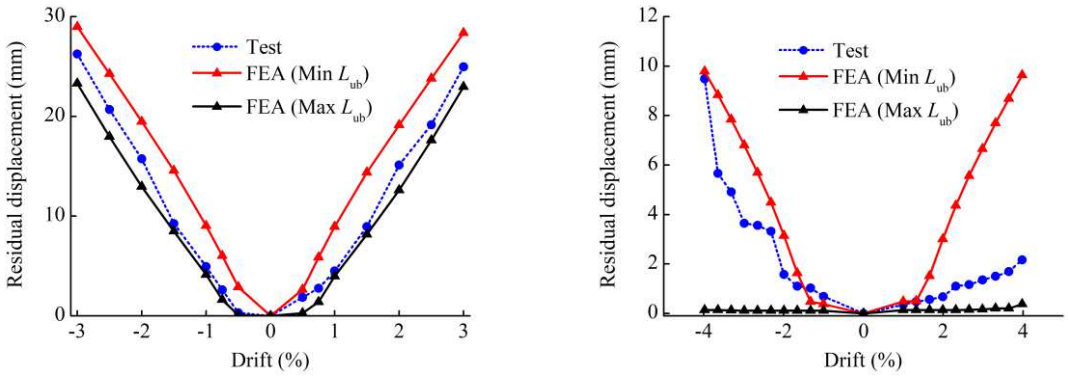

(a) HBD1 (b) s-SCP(I-ED)

Fig. 3 Comparison of the numerical residual displacement with the test results

Based on the above analysis and Fig. 3, it can be concluded that the proposed simulation method is effective. However, there is uncertainty of L_{ub} in the modeling process, a conservative result of residual displacement will be obtained generally if the

strain penetration is not considered, and it is highly possible to underestimate the residual displacement if using Eq. (3) to calculate the equivalent unbonded length.

3. Governing design parameters for residual displacement

Two design parameters, the SC factor and ED parameter, are believed to have governing influence on the residual displacement.

3.1 Definition and calculation of SC factor

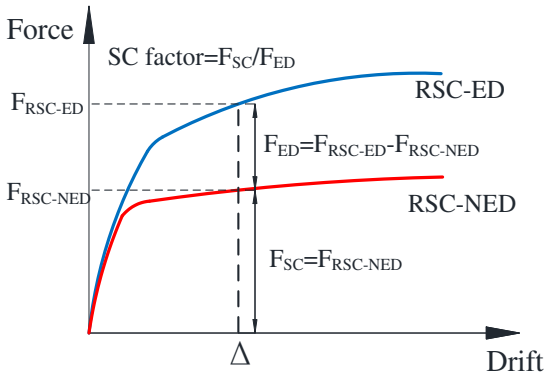

Fig. 4 Definition and calculation of SC factor

Several researchers have put forward different SC factor for evaluating the self-centering capacity of RSC columns. Hieber et al. (2005) proposed the re-centering ratio which is equal to the ratio between the total axial force (including the gravity force and initial prestressing force) and the yielding force of ED bars. The self-centering capacity of bridge columns at different drifts is usually different, while the re-centering ratio is a constant for an RSC column.

The contribution ratio λ_{SC} is another SC factor and it is typically adopted in the design of RSC systems (Palermo et al. 2007; Wang et al. 2019; Weng et al. 2010). λ_{SC} in its generic form represents the force or moment ratio between the self-centering contribution and the energy dissipation contribution, as shown in Eq. (7).

$$\lambda_{SC} = \frac{M_{\text{self-centering}}}{M_{\text{dissipation}}} = \frac{F_{\text{self-centering}}}{F_{\text{dissipation}}} \tag{7}$$

The self-centering and energy dissipation contribution can be derived from the monolithic beam analogy procedure (Pampanin et al. 2001). However, the iterative calculation process is still relatively complicated. What's more, λ_{SC} is obtained from theoretical calculation, while the residual displacement is determined by simulation. In order to reduce error, it is better that using simulation method to measure the self-centering performance index. For this reason, the SC factor λ_{SC} used in this study is defined as follows:

$$\lambda_{SC} = \frac{F_{SC}}{F_{ED}} \tag{8}$$

where F_{SC} is the self-centering contribution provided by gravity load and PT tendons, and F_{ED} is the energy dissipation contribution provided by ED bars. As shown in Fig. 4, the calculation of λ_{SC} requires the following two steps:

(1) Establish the numerical model of RSC-ED columns and conduct a pushover analysis, then the force-displacement curve can be obtained. The force $F_{\text{RSC-ED}}$ includes the self-centering and energy dissipation contribution.

(2) Delete the ED bar elements from the existing numerical model of the RSC-ED column and perform a pushover analysis again, then the force-displacement curve which only contain the self-centering contribution is obtained. Therefore, the energy dissipation contribution F_{ED} can be derived as:

$$F_{ED} = F_{\text{RSC-ED}} - F_{\text{RSC-NED}} \tag{9}$$

3.2 Definition and calculation of ED parameter

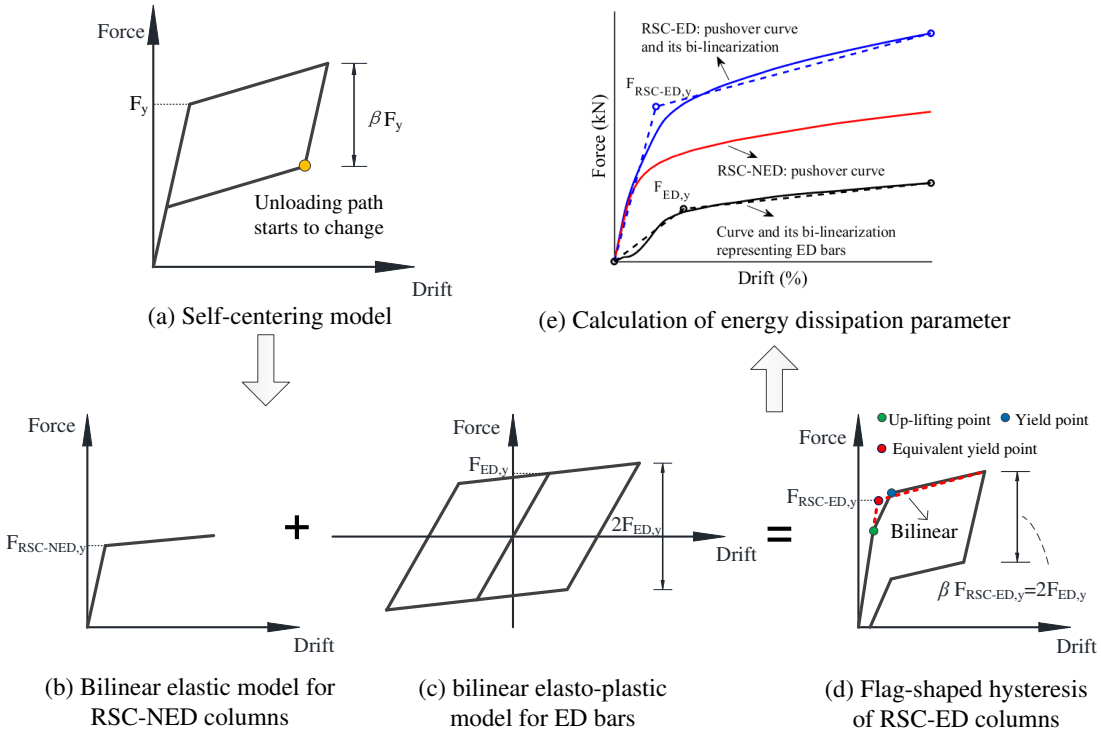

Fig. 5 Definition and calculation of ED parameter

The second governing design parameter is ED parameter. The cyclic behavior of RSC columns can be simplified into a flag-shaped hysteretic model as shown in Fig. 5(a). The ED parameter β is a significant parameter in this model, it not only reflects the energy dissipation capacity of the model, but also controls the where the unloading path starts to change. The smaller the ED parameter is, the earlier the unloading path changes, leading to smaller residual displacement. Hence, it can be predicted that the ED parameter has a non-ignorable influence on the residual displacement, while the recent researches related to the residual displacement of RSC systems all did not consider it.

The self-centering model is so ideal that it is unable to capture the residual displacement in fact. Implementing two rotational springs in parallel with appropriate hysteretic models is another simplified simulation method. The RSC column without

ED bars is modelled by a bilinear elastic model, as shown in Fig.5 (b). The ED bar is simulated using a bilinear elasto-plastic model, as shown in Fig.5 (c). With the coaction of the two springs, the RSC column presents a trilinear skeleton curve to be exact, there is a stiffness reduction after the column is lifted up. Since the stiffness reduction is very slight, the skeleton curve can be approximate to a bilinear one.

To extract the ED parameter, an equivalent linearization method is used. The ED parameter can be calculated as:

$$\beta = \frac{2F_{ED,\mathrm{y}}}{F_{\mathrm{RSC\text{-}ED,y}}} \tag{10}$$

where $F_{\mathrm{ED,y}}$ is the yielding force of the bilinear elasto-plastic model; $F_{\mathrm{RSC\text{-}ED,y}}$ is the effective yielding strength of the bridge column, as shown in Fig. 5(d).

Eq. (10) can be expressed approximately as:

$$\beta \approx \frac{2F_{ED,\mathrm{y}}}{F_{ED,\mathrm{y}} + F_{\mathrm{RSC\text{-}NED,y}}} = \frac{2}{1 + F_{\mathrm{RSC\text{-}NED,y}} / F_{ED,\mathrm{y}}} = \frac{2}{1 + \lambda_{\mathrm{SC,y}}} \tag{11}$$

where $F_{\mathrm{RSC\text{-}NED,y}}$ is the yielding force of the bilinear elastic model, $\lambda_{\mathrm{SC,y}}$ is the SC factor that corresponds to the yield displacement. It can be found that the value of β is relatively stable, and it is smaller than 1 when the value of $\lambda_{\mathrm{SC,y}}$ exceeds 1. As shown in Fig. 5(e), the calculation of β requires the following two steps:

(1) Establish the FE model of an RSC-ED column and perform a pushover analysis, then the obtained pushover curve is bilinearized according to the equal energy principle, the parameter $F_{\mathrm{RSC\text{-}ED,y}}$ can be determined.

(2) Delete the ED bar elements from the FE model and carry out a pushover analysis again, then the force-displacement curve representing the energy dissipation

contribution can be plotted by subtraction. Conduct an equivalent linearization again and the parameter $F_{ED,y}$ is obtained.

4. Fractional factorial analysis

In the actual construction of RSC columns, the key design parameters are presented in the form of aspect ratio λ, concrete strength f_c, PT tendon ratio ρ_{PT}, axial-load ratio (η_G, η_{PT}) caused by gravity load P_G and PT force P_{PT}, ED bar ratio ρ_{ED}, yield stress of ED bars f_y and unbonded length L_0. It should be noted that the non-dimensional parameters, the SC factor and ED parameter, can be regarded as the comprehensive embodiment of these key design parameters. This part of study uses fractional factorial analysis to discuss the effect of each parameter on the SC factor and ED parameter at different drifts.

4.1 Design parameters of reference specimen

In the factorial analysis study, the reference specimen RS chooses the prototype of specimen HBD1, the specimen HBD1 is 1/3 scaled, but the design parameters of specimen RS are not strictly converted by a scale of 1:3 according to those of specimen HBD1, as shown in Table 2. For example, in order to ensure the ED bars have enough deformation capacity at larger loading drift, the value of L_0 of the specimen RS is set to 300 mm rather than 150 mm. The prototype pier of specimen HBD1 has a total mass of 180 t, but the gravity force was not applied in the test due to the limitation of the experimental prestressing, the value of P_G of the specimen RS is 1800 kN. Meanwhile, P_G will enhance the self-centering capacity of the specimen RS, which may lead to no residual displacement. Therefore, the value of P_{PT} is set to 600 kN rather than 1800

kN.

Table 2 Comparison of the design parameters of specimens HBD1 and RS

Specimen	Width (mm)	λ	f_c (MPa)	ED bar	ρ_{ED} (%)	f_y (MPa)	L_0 (mm)	PT tendon	ρ_{PT} (%)	P_G (kN)	η_G	P_{PT} (kN)	η_{PT}
HBD1	350	4.57	54.1	4D16	0.66	304	50	2×99 mm^2	0.16	0	0	200	0.03
RS	1050	4.57	54.1	20D22	0.69	304	300	12D15.2	0.2	1800	0.03	600	0.01

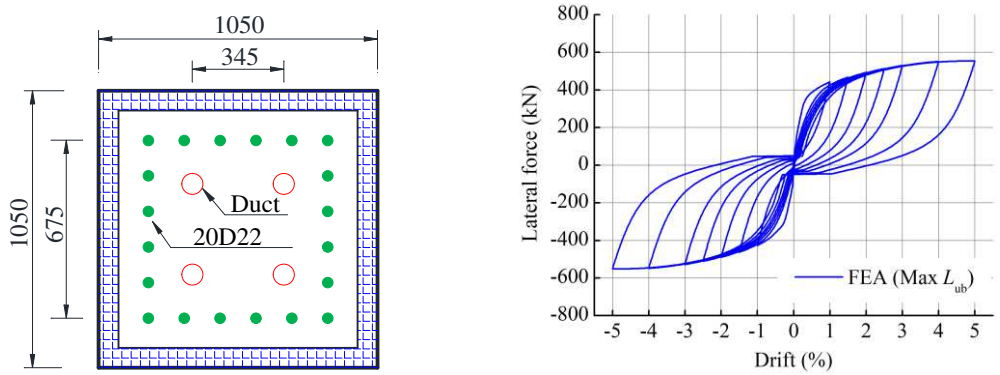

(a) Cross-section (b) hysteretic curve

Fig. 6 Cross-section and cyclic behavior of specimen RS (Unit: mm)

Fig. 6(a) shows the cross-section of the specimen RS, each duct holds 4 PT tendons, and the diameter and tensile strength of each PT tendon are 15.2 mm and 1860 MPa, respectively. The PT tendon ratio can be easily adjusted by changing the number of PT tendons in each duct, the ED bar ratio can be changed by altering the diameter of ED bars in the following study. The hysteretic curve of the specimen RS is plotted in Fig. 6(b). For specimen HBD1, the simulation result corresponding to the maximum value of L_{ub} matches better with the test result, as shown in Fig. 2(c), so the maximum L_{ub} is adopted in this part.

4.2 Two-level fractional design

The purpose of of this fractional factorial analysis is to evaluate the importance of the key design parameters to the residual displacement of RSC columns. Table 3 shows the key parameters and the two levels of each parameter. The ranges of the factors are

305 determined by the investigation of 19 RSC column specimens (Palermo et al. 2007; Ou
306 et al. 2010; Tong et al. 2019; Bu et al. 2016; Marriott et al. 2009), the statistical results
307 are also reported in Table 3. To prevent the PT tendon yields under cyclic loading, the
308 value of P_d corresponding to its high level is set to 0.4, and the maximum loading drift
309 is 4%.

310 Factorial analysis is used often when multiple factors exist in determining an
311 output. However, the full factorial analysis requires a great number of runs if many
312 factors are taken into account, which may become computationally expensive. In this
313 study, the analysis includes eight factors and each factor has two levels, a complete
314 factorial analysis needs 256 runs. In order to improve the efficiency, one-eighth factorial
315 analysis is performed, which decreased the required runs to 2^{8-3} for a total of 32.

316 The approach Montgomery proposed (2008) is used to perform the fractional
317 factorial analysis. The construction of a one- eighth factorial analysis consists of two
318 parts. The first part is a basic design, which contains a complete 2^{8-3} fractional factorial
319 combination (the first five columns in Table 4). The other part includes three generators
320 (the last three columns in Table 4) which determines the factors that are not included in
321 the basic design. – and + are the symbols of low level and high level, respectively. The
322 levels of the last three factors are determined by using generating relations.

323 Table 3 Two levels of the considered factors

Level	λ (A)	f_c (B)	P_d (C)	ρ_{PT} (D)	η_G (E)	L_0 (mm) (F=ABC)	f_y (MPa) (G=ABD)	ρ_{ED} (H=BCDE)
Range	4.42~5.29	32~65.9	0.12~0.51	0.13%~0.65%	0~0.1	50~400	300~600	0.26%~1.03%
- (low)	3.5	30	0.2	0.20%	0.02	150	300	0.46%
+ (high)	6	60	0.4	0.60%	0.1	450	600	1.12%

324 Note: P_d is the ratio between the initial stress of a PT tendon and its yield stress.

Table 4 2^{8-3} fractional factorial design

Case (Level)	Basic design					Generated from basic design		
	λ (A)	f_c (B)	P_d (C)	ρ_{PT} (D)	η_G (E)	L_0 (F=ABC)	f_y (G=ABD)	ρ_{ED} (H=BCDE)
1	-1	-1	-1	-1	-1	-1	-1	1
2	1	-1	-1	-1	-1	1	1	1
3	-1	1	-1	-1	-1	1	1	-1
4	1	1	-1	-1	-1	-1	-1	-1
5	-1	-1	1	-1	-1	1	-1	-1
6	1	-1	1	-1	-1	-1	1	-1
7	-1	1	1	-1	-1	-1	1	1
8	1	1	1	-1	-1	1	-1	1
9	-1	-1	-1	1	-1	-1	1	-1
10	1	-1	-1	1	-1	1	-1	-1
11	-1	1	-1	1	-1	1	-1	1
12	1	1	-1	1	-1	-1	1	1
13	-1	-1	1	1	-1	1	1	1
14	1	-1	1	1	-1	-1	-1	1
15	-1	1	1	1	-1	-1	-1	-1
16	1	1	1	1	-1	1	1	-1
17	-1	-1	-1	-1	1	-1	-1	-1
18	1	-1	-1	-1	1	1	1	-1
19	-1	1	-1	-1	1	1	1	1
20	1	1	-1	-1	1	-1	-1	1
21	-1	-1	1	-1	1	1	-1	1
22	1	-1	1	-1	1	-1	1	1
23	-1	1	1	-1	1	-1	1	-1
24	1	1	1	-1	1	1	-1	-1
25	-1	-1	-1	1	1	-1	1	1
26	1	-1	-1	1	1	1	-1	1
27	-1	1	-1	1	1	1	-1	-1
28	1	1	-1	1	1	-1	1	-1
29	-1	-1	1	1	1	1	1	-1
30	1	-1	1	1	1	-1	-1	-1
31	-1	1	1	1	1	-1	-1	1
32	1	1	1	1	1	1	1	1

4.3 Results of factorial analysis

Based on the earthquake damage investigation results, the Japan Road Association (JRA) code proposed a residual drift limitation of 1% for RC columns to measure whether the columns could be repaired or not (Japan Road Association, 2002). If the

residual drift does not exceed 1%, the damaged column can be repaired generally. Due to the residual drift is always smaller than the peak drift, the SC factor and ED parameter at 1% drift are not concerned.

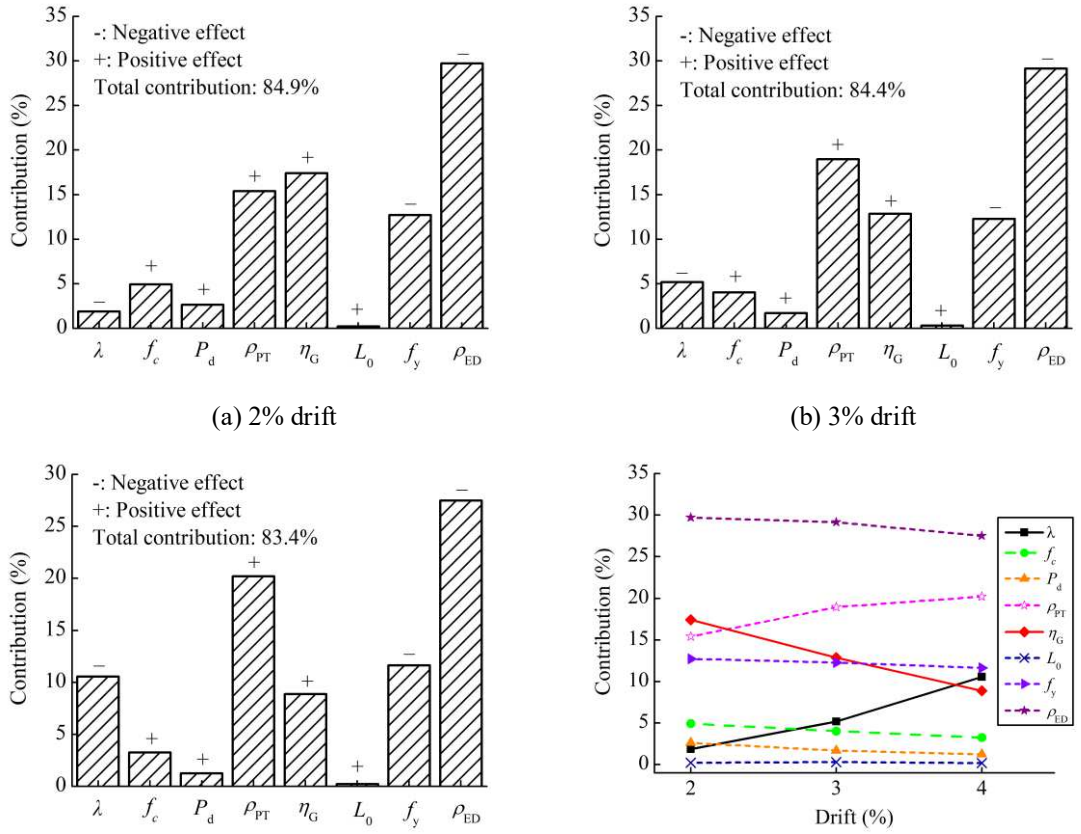

(a) 2% drift (b) 3% drift

(c) 4% drift (d) Change of contribution

Fig. 7 Contribution of key parameters to SC factor under different drifts

The effect of each key parameter on the SC factor at 2%, 3% and 4% drift is compared as shown in Fig. 7. Except for λ, f_y and ρ_{ED}, the else five parameters have positive influence on the SC factor. At the considered levels of the parameters, the most important parameters is ρ_{ED}, f_y, ρ_{TP} and η_G, the contribution of L_0 can be neglected. The change of contribution provided by each parameter is presented in Fig. 7(d), it can be be observed that the change of the contribution provided by λ and η_G is the most notable. With the increase of drift, the contribution of λ increases from 1.9%

to 10.5%, while the contribution of η_G declines from 17.4% to 8.9%. This is because the larger aspect ratio and drift will aggravate the P-Δ effect. Meanwhile, the contribution of ρ_{TP} grows about 5%, which indicates the self-centering capacity is more dependent on ρ_{TP} at large drift. The total contribution is very stable and exceeds 83% no matter which drift is considered, no intense interaction between the parameters is observed.

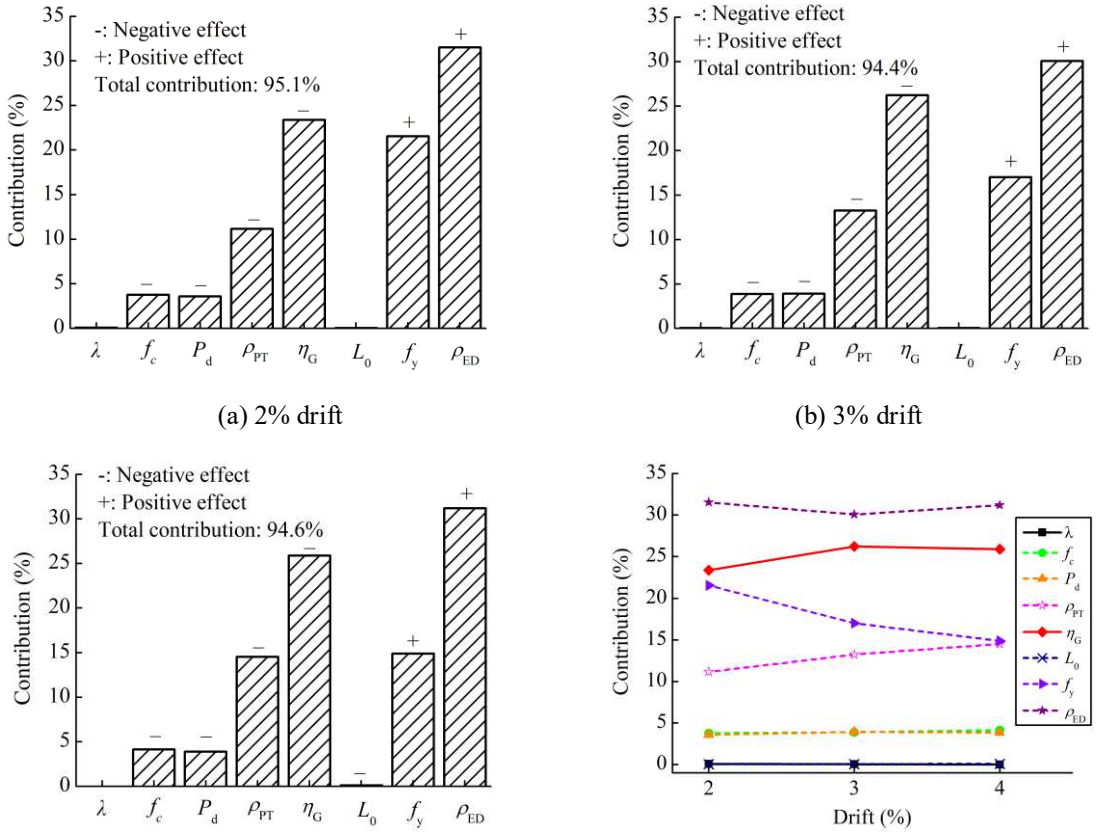

(a) 2% drift (b) 3% drift

(c) 4% drift (d) Change of contribution

Fig. 8 Contribution of key parameters to ED parameter under different drifts

As shown in Fig. 8, the contribution of each factor to the ED parameter at 2%, 3% and 4% drift is compared. f_c, P_d, ρ_{TP} and η_G have a negative effect, f_y and ρ_{ED} have a positive effect, the effect of λ and L_0 is approximate to zero. The most significant parameters are ρ_{ED}, f_y, η_G and ρ_{TP}. As shown in Fig. 8(d), the contribution of these parameters excluding f_y basically remains the same, the

contribution of f_y decreases from 21.5% to 14.9% as the drift increases from 2% to 4%. On the other hand, the total contribution at the three loading drifts all reaches 94%, it can be concluded that the ED parameter is dominated by the effect of single factor and the interaction between the factors is very slight. Here, the ED parameter β is fitted with a linear regression model which can be expressed as follows:

$$\beta = a_0 + a_1 x_1 + a_2 x_2 + a_3 x_3 + a_4 x_4 + a_5 x_5 + a_6 x_6 \tag{12}$$

where x_1, x_2, x_3, x_4, x_5 and x_6 are the normalized parameters representing the effect of f_c, P_d, ρ_{TP}, η_G, f_y and ρ_{ED}. For example, $x_1 = (\lambda - 45)/15$. The normalized parameters range from -1 to 1 (corresponding to low and high levels). The obtained corresponding coefficients of the regression model are given in Table 5.

Table 5 Coefficient values of the regression model for β

Drift	Coefficients						
	a_0	a_1	a_2	a_3	a_4	a_5	a_6
2%	0.760	-0.062	-0.060	-0.106	-0.154	0.148	0.179
3%	0.749	-0.062	-0.062	-0.115	-0.161	0.130	0.173
4%	0.746	-0.063	-0.061	-0.118	-0.157	0.119	0.173

5. Formula to predict residual drift under cyclic loading

The purpose of this part is exploring the effect of the SC factor and ED parameter on the distribution of the residual drift, and predicting the residual drift under cyclic loading. Due to there are two directions during a full cycle, the residual drift D_{res} is defined as:

$$D_{res} = \frac{D_{-res} + D_{+res}}{2} \tag{13}$$

where D_{-res} and D_{+res} are the residual drift corresponding to the negative and positive loading directions, respectively.

5.1 Parametric study

In order to obtain enough data to analyze the distribution of residual drift, a parametric study is first carried out. Table 6 shows the all the specimens used in the parametric study, the specimens are designed based on the specimen RS. Each specimen has a special denotation which corresponding to a value of the parameter. For example, for the aspect ratio λ, five specimens are designed and tagged with A1, A2, A3, A4 and A5. Among these tags, A1 corresponds to a value of 3.6.

Table 6 Denotation of specimens in parametric study

Parameters	Denotation	Parameter values for each specimen
λ	A1, A2, A3, A4, A5 (A1-A5)	3.6, 4.6, 5.5, 6.5, 7.4
P_d	PD1, PD2, PD3, PD4, PD5, PD6 (PD1-PD6)	0.15, 0.2, 0.3, 0.4, 0.5, 0.6
ρ_{PT}	PT1, PT2, PT3, PT4, PT5, PT6 (PT1-PT6)	0.13%, 0.2%, 0.26%, 0.33%, 0.4%, 0.53%
η_G	G1, G2, G3, G4, G5 (G1-G5)	0.03, 0.045, 0.06, 0.075, 0.091
L_0	L1, L2, L3, L4, L5 (L1-L5)	300 mm, 400 mm, 500 mm, 600 mm, 700 mm
f_y	F1, F2, F3, F4, F5 (F1-F5)	304 MPa, 350 MPa, 400 MPa, 450 MPa, 500 MPa
ρ_{ED}	E1, E2, E3, E4, E5, E6 (E1-E6)	0.46%, 0.69%, 0.89%, 1.12%,1.46%, 2.28%

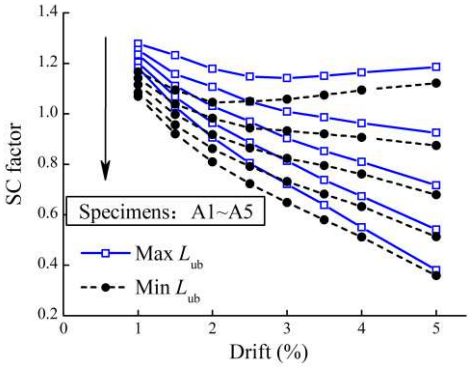

(a) Aspect ratio

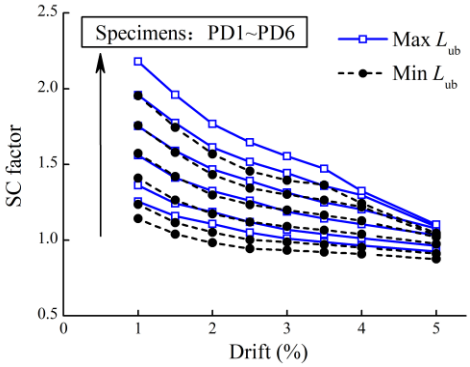

(b) Ratio between initial stress and yield stress

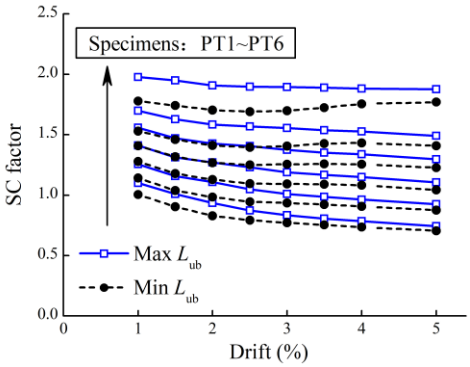

(c) PT tendon ratio

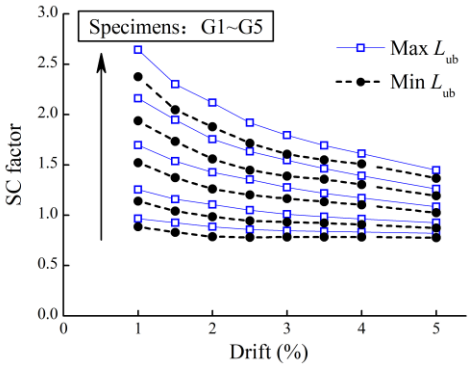

(d) Gravity axial load

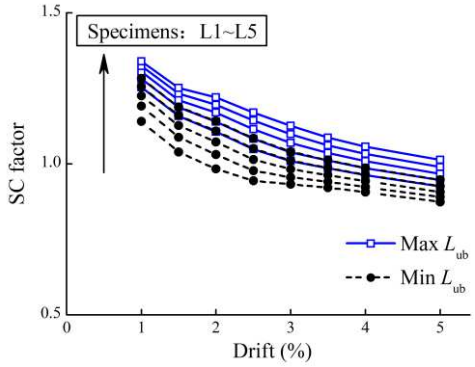

(e) Unbonded length of ED bars

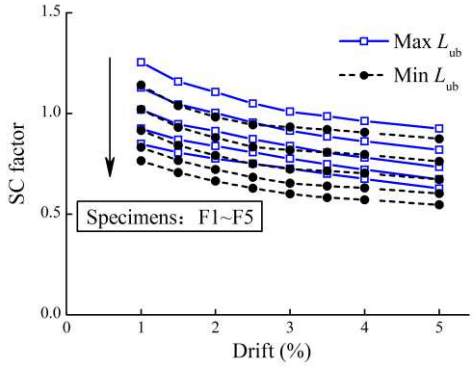

(f) Yield stress of ED bars

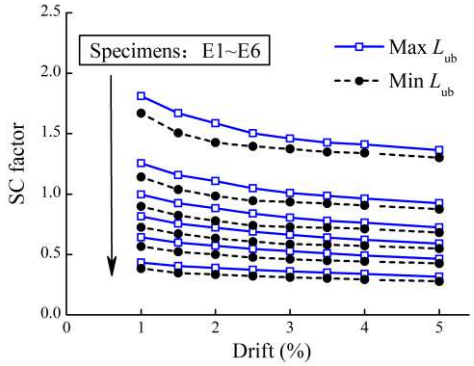

(g) ED bar ratio

Fig. 9 Influence of each parameter on SC factor

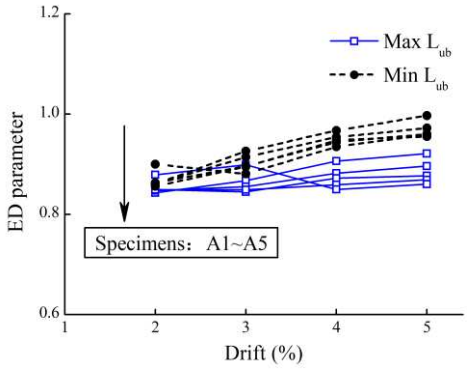

(a) Aspect ratio

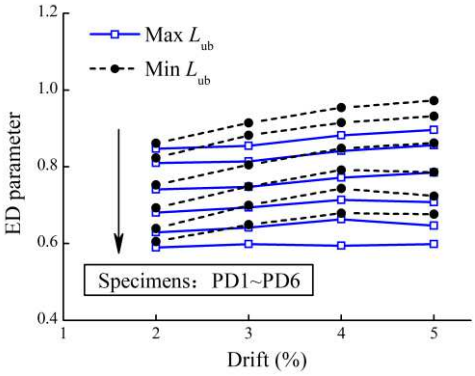

(b) Ratio between initial stress and yield stress

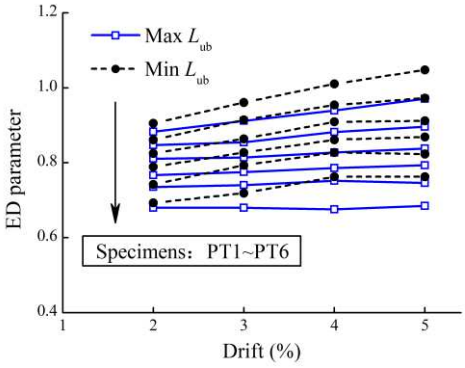

(c) PT tendon ratio

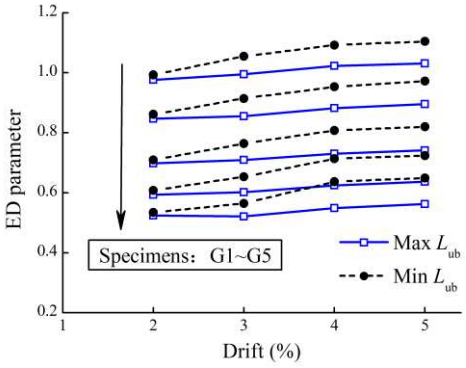

(d) Gravity axial load

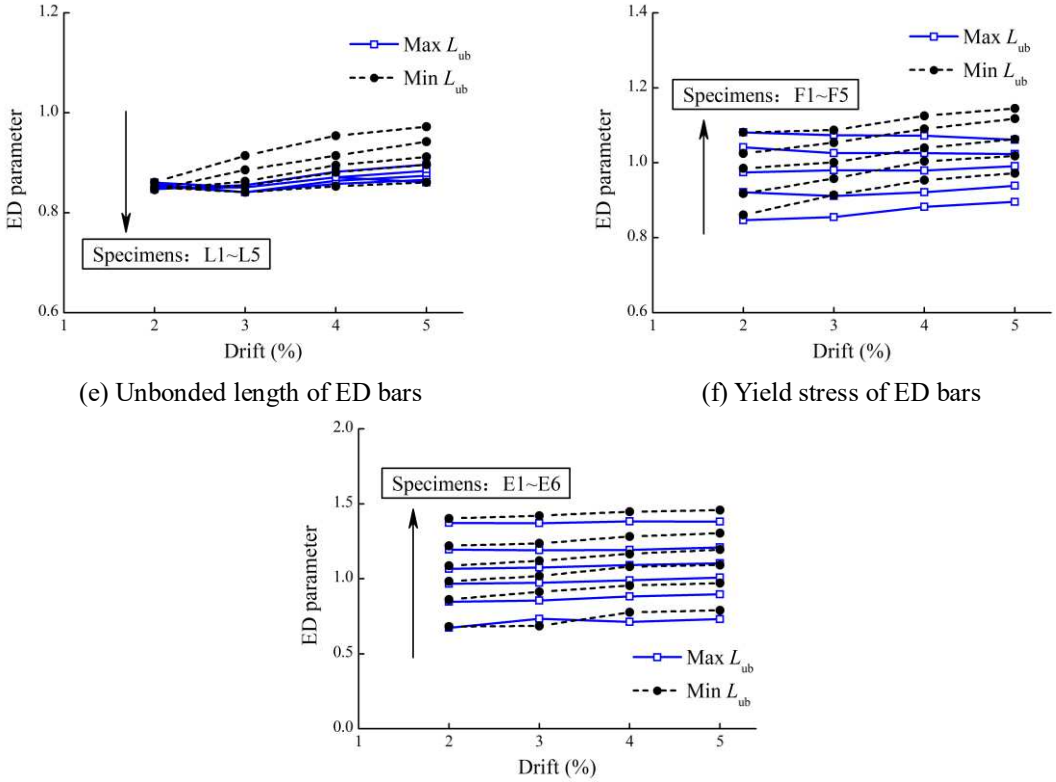

(e) Unbonded length of ED bars

(f) Yield stress of ED bars

(g) ED bar ratio

Fig. 10 Influence of each parameter on ED parameter

Fig. 9 shows the influence of each parameter on the SC factor, the uncertainty of L_{ub} in the simulation process is considered. It can be concluded that the value of the SC factor corresponding to minimum L_{ub} is always smaller than that corresponding to maximum L_{ub}, which indicates that the self-centering capacity of bridge columns will be underestimated if the strain penetration is not considered. The uncertainty of L_{ub} has little influence on the change tendency of the SC factor, the SC factor presents a downward trend as the drift increases.

As shown in Fig. 9(a), the five specimens (A1-A5) have a similar SC factor at 1% drift. With the increase of drift, the SC factor of the specimen with a larger aspect ratio descends more rapidly because of the P-Δ effect. Specimen A1 is different from other specimens, its SC factor has a slight growth when the drift exceeds a certain value.

Increasing P_d, ρ_{PT}, η_G and L_0 are all benefit to improve the self-centering force, so their increase will enhance the SC factor as shown in Fig. 9(b), (c), (d) and (e). The improvement effect of P_d and η_G on the SC factor is very similar and dependent on the drift as shown in Fig. 9(b) and (d), a larger P_d and η_G can generate a larger SC factor generally, but the self-centering capacity is not stable, which decreases sharply at the drift increases. As shown in Fig.9 (c), it can be concluded that increasing the PT tendon ratio is an effective method to strength the stability of the self-centering capacity. Compared to P_d, ρ_{PT} and η_G, the effect of L_0 on the SC factor is very limited as shown in Fig.9 (e). The value of L_0 increase from 300 mm to 700 mm, while the increase of SC factor does not exceed 0.3. Increasing f_y or ρ_{ED} is helpful to improve the energy dissipation capacity, so their increase will reduce the SC factor as shown in Fig. 9(f) and (g). There is a greatest reduction of the SC factor when ρ_{ED} increases from 0.46% to 0.69% as shown in Fig. 9(g).

Similarly, Fig. 10 shows the influence of each parameter on the ED parameter, it can be observed that the ED parameter corresponding to the minimum L_{ub} is larger than that corresponding to the maximum L_{ub} commonly. With the increase of drift, the ED parameter shows a slight uptrend, it keeps stable on the whole and its largest growth does not reach 0.2. As shown in Fig. 10(a), (b), (c), (d) and (e), increasing λ, P_d, ρ_{PT}, η_G and L_0 are able to reduce the ED parameter, especially for η_G, P_d and ρ_{PT}, their reduction effect is more remarkable, and the effect of λ and L_0 is relatively limited. Increasing f_y and ρ_{ED} are capable of improve the ED parameter as shown in Fig. 10(f) and (g).

5.2 Regression analysis

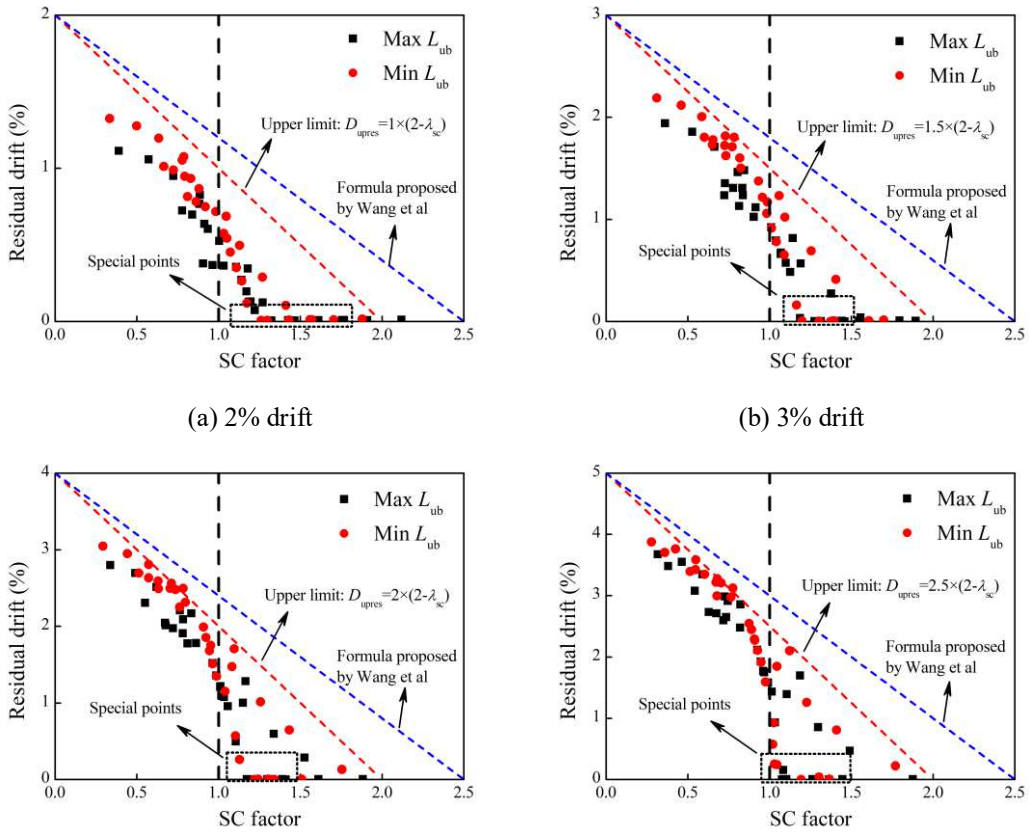

(a) 2% drift (b) 3% drift

(c) 4% drift (d) 5% drift

Fig. 11 Effect of SC factor on residual drift distribution

As shown in Fig.11, the data obtained from the parameter analysis are collected to investigate the influence of the SC factor on the residual drift distribution. The black points correspond to the maximum L_{ub} and the red points corresponds to the minimum L_{ub}. The red points are located at the upper boundary of the black points. The upper limit of the residual drift is dominated by two key coordinate points which are (2, 0) and (0, D_{max}). Point (2, 0) indicates that the residual drift is equal to zero if the SC factor reaches 2; point (0, D_{max}) indicates that the residual drift is equal to the maximum drift if the SC factor is 0. The upper limit of residual drift D_{upres} at different drifts can be expressed as Eq. (14). Wang et al. (2019) proposed a formula for the RSC UHPC bridge

column with a hollow section to calculate the upper limit of residual drift, as shown in Eq. (15). Eq. (14) is very similar to Eq. (15), the only difference is that Eq. (15) believes the residual drift is equal zero when the SC factor is 2.5. Therefore, Eq. (15) is more conservative as shown in Fig. 11. However, it does not mean that the concrete material or the section shape have great influence on the upper limit of residual drift. In (Wang et al. 2019), the SC factor defined as the moment contribution ratio is obtained by theoretical calculation, while the residual drift is obtained from the numerical results, which will amplify the error.

$$D_{\text{upres}} = D_{\max} \times (1 - 0.5\lambda_{\text{SC}}) \tag{14}$$

$$D_{\text{upres}} = D_{\max} \times (1 - 0.4\lambda_{\text{SC}}) \tag{15}$$

In addition, the residual drift exhibits a feature of linear distribution. However, there are some special points the SC factors of which exceed 1, while the corresponding residual drift is very small and approximate to zero. These special points show an entirely different pattern of distribution. In order to explain the phenomenon, the source of these special points is checked, finding most of them are obtained from the specimens PD1-PD6, PT1-PT6, and G1-G5. P_{d}, ρ_{PT} and η_{G} all have great negative effect on the ED parameter, so the influence of the ED parameter on the residual drift distribution is studied as shown in Fig. 12. When the ED parameter exceeds 0.75, the residual drift is very sensitive to it, especially within the range of 0.75 to 1.0, the residual drift grows rapidly as the ED parameter increases; when the ED parameter exceeds 1.0, the residual drift increases in a smooth way. Meanwhile, the distribution of residual drift is stratified because the residual drift depends heavily on the maximum

475 drift. On the other hand, it can be concluded that the residual drift is close to zero when
476 the ED parameter is less than 0.75, which is not related to the maximum drift.

477 As shown in Fig.13, the data in Fig.11 are collected and the points of which the ED
478 parameter is larger than 0.75 are removed. It can be found that the most of the special
479 points are filtered out, and the filtered data exhibit a more obvious linear distribution
480 characteristic. Regression analyses are performed for the filtered data, and the relation
481 between the residual drift at a certain drift and the SC factor is established as follows:

482 $$D_{\mathrm{res},2\%} = -1.4\lambda_{\mathrm{SC}} + 1.936 \tag{16a}$$

483 $$D_{\mathrm{res},3\%} = -1.972\lambda_{\mathrm{SC}} + 2.974 \tag{16b}$$

484 $$D_{\mathrm{res},4\%} = -2.515\lambda_{\mathrm{SC}} + 3.973 \tag{16c}$$

485 $$D_{\mathrm{res},5\%} = -3\lambda_{\mathrm{SC}} + 4.9 \tag{16d}$$

486 where $D_{\mathrm{res},2\%}$, $D_{\mathrm{res},3\%}$, $D_{\mathrm{res},4\%}$, and $D_{\mathrm{res},5\%}$ were the residual drifts at 2, 3, 4, and 5%
487 drift. It should be noted the set of formula can be used to estimate the residual drift
488 under cyclic loading on the premise that the ED parameter exceeds 0.75. If the
489 parameter is smaller than 0.75, the residual drift can be ignored. The correlation
490 coefficients of Eq. (16a), Eq. (16b), Eq. (16c), Eq. (16d) are 86.6%, 85.6%, 85.4%
491 and 84.8%, respectively.

492 Too large value of L_0 is an important reason leading to the discreteness of the
493 formulas. As shown in Fig.13, there are lots of points descend faster as the SC factor
494 increases, this is because too large value of L_0 will change the unloading path and
495 aggravates the pinching effect, meanwhile, the SC factor is not sensitive to L_0. As a
496 result, the residual drift is reduced at the cost of a slight reduction in strength and energy

dissipation capacity. A Comparison of the hysteretic curves between specimen L1 and L5 are given as an example, as shown in Fig.14. In fact, a too long unbonded length will not be designed generally due to it may lead to the buckling of ED bars, so it is unnecessary to pay much attention on the effect of L_0.

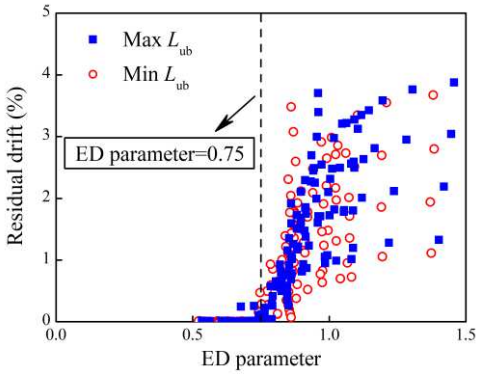

Fig. 12 Effect of ED parameter on residual drift distribution

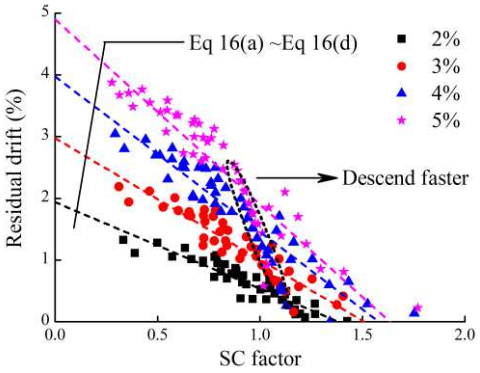

Fig. 13 Regression analysis

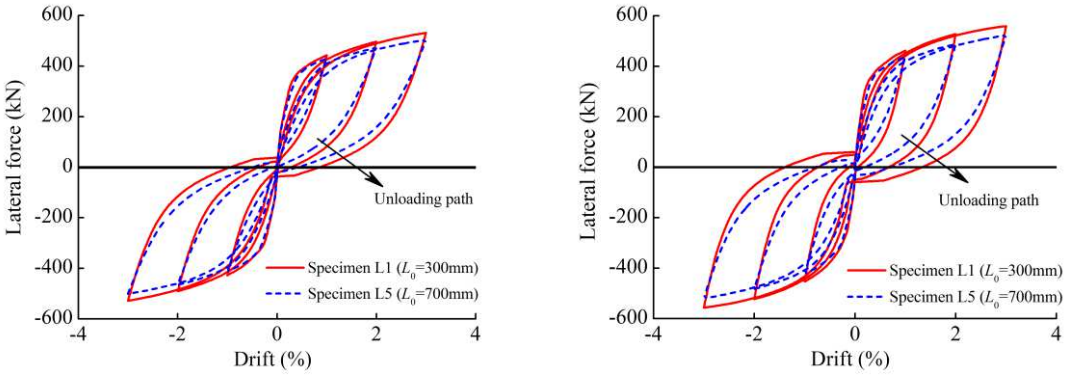

(a) Maximum L_{ub} (b) Minimum L_{ub}

Fig. 14 Comparison of hysteretic curves between specimen L1 and L5

Palermo et al. (2007) conducted a cyclic loading test on four RSC bridge pier specimens. There specimens were named PT1, HBD1, PT2 and HBD2, the only different between specimen PT1 (PT2) and HBD1 (HBD2) is the former lacks of ED bars. The SC factors and ED parameters of specimen HBD1 and HBD2 can be obtained from the test results. A comparison of the test results with the predictive residual drift is given as shown in Table 7.

512 Table 7 Comparison of the test results with predictive results

Specimens	Drift	SC factor	ED parameter	Residual drift (%)		
				Test	Upper limit	Predictive result
HBD1	2%	1	0.98	0.94	1	0.54
	3%	0.98	0.97	1.55	1.53	1.04
HBD2	2%	1.4	0.83	0.23	0.6	0

513 # 6. Conclusion

514 This paper uses numerical method to investigate and predict the residual
515 displacement of RSC columns under cyclic loading. The SC factor and ED parameter
516 are regarded as the important parameters to govern the residual displacement. The
517 contribution of eight design parameters at different drifts is discussed by factorial
518 analysis. The effect of the SC factor and ED parameter on the residual drift distribution
519 is analyzed statistically. During the process, the uncertainty of L_{ub} in numerical model is
520 considered. Finally, a set of predictive formulas is proposed by regression analyses.

521 Based on the analyses, the following conclusions can be drawn:

522 (1) Ignoring the strain penetration of ED bars will underestimate the self-centering
523 capacity of RSC columns, and conservative residual displacement will be obtained.

524 (2) The total contribution of the eight parameters to the SC factor and ED parameter are
525 stable and maintain at 84% and 95% around, respectively. No significant interaction
526 between these factors is observed. Due to the P-Δ effect, the contribution of the gravity
527 loading ratio to the SC factor will decreases rapidly as the drift increase, and the effect
528 of the aspect ratio will grow.

529 (3) The SC factor, ED parameter, and maximum drift dominate the distribution of
530 residual drift under cyclic loading. When the SC factor exceeds 2.0 or the ED parameter
531 is smaller than 0.75, the residual drift can be neglected. In other situations, the residual

drift can be estimated using the upper limit formula and the regression formula.

(4) The unbonded length of ED bars has little influence on the SC factor and the ED parameter. However, if the unbonded length is too long, the residual displacement can be diminished effectively because of the changed unloading path.

Declarations

Funding This work is supported by National Natural Science Foundation of China (Grant No. 51908265 and No. 52008186) and Fund for Excellent Young Scholars of LUT (Grant No. 04-061810).

Conflict of interest The authors declare that they have no known competing financial interests or personal relationships that could have appeared to influence the work reported in this paper.

Availability of data and material Not applicable.

Code availability Not applicable.

Authors' contributions Yan Shi and Zhengwu Zhong contributed to the modelling and the analysis of the numerical results. The first draft of the manuscript was written by Zhengwu Zhong, with the contribution of Zhichao Zhang for the editing of the figures and tables. Yan Shi, Jianping Han and Hu Cheng participated in the review of the document and read and approved the final manuscript.

Reference

[1] Han Q, Du X, Liu J, et al. Seismic damage of highway bridges during the 2008 Wenchuan earthquake[J]. Earthquake Engineering & Engineering Vibration 2009;8(2):263–73.

[2] Shi Y, Zhong Z, Qin H, et al. Toggle buckling-restrained brace systems and a corresponding design method for the seismic retrofit of bridge bents[J]. Engineering Structures, 2020, 221:110996.

[3] Kawashima K, Macrae G A, Hoshikuma J I, et al. Residual drift response spectrum[J]. Journal of Structural Engineering, 1998, 124(5):523-530

[4] Uma SR, Pampanin S, Christopoulos C. Development of probabilistic framework for

559 performance-based seismic assessment of structures considering residual deformations[J].
560 Journal of Earthquake Engineering, 2010,14(7):1092–1111.
561 [5] Palermo A, Mashal M. Accelerated bridge construction (ABC) and seismic damage resistant
562 technology: A New Zealand challenge[J]. Bulletin of the New Zealand Society for Earthquake
563 Engineering, 2012, 45(3): 123-134.
564 [6] Marsh M L, Wernli M, Garrett B E, et al. Application of accelerated bridge construction
565 connections in moderate-to-high seismic regions, NCHRP Report 698[R]. Transportation
566 Research Board, Washington, DC, USA, 2011.
567 [7] Hewes J T, Priestley M J N. Seismic design and performance of precast concrete segmental
568 bridge columns (No.SSRP-2001/25)[R]. University of California at SanDiego, 2002.
569 [8] Palermo A, Pampanin S, Marriott D. Design, modeling, and experimental response of seismic
570 resistant bridge piers with posttensioned dissipating connections[J]. Journal of Structural
571 Engineering, 2007, 133(11): 1648-1661.
572 [9] Ou Y, Wang P, Tsai M S, et al. Large-scale experimental study of precast segmental unbonded
573 posttensioned concrete bridge columns for seismic regions[J]. Journal of Structural Engineering,
574 2010, 136(3): 255-264.
575 [10] Bu Z, Ou Y, Song J, et al. Cyclic loading test of unbonded and bonded posttensioned precast
576 segmental bridge columns with circular section[J]. Journal of Bridge Engineering, 2016, 21(2):
577 04015043
578 [11] Elgawady M A, Sha'lan A. Seismic behavior of self-centering precast segmental bridge bents[J].
579 Journal of Bridge Engineering, 2011, 16(3): 328-339.
580 [12] Guo T, Cao Z, Xu Z, et al. Cyclic load tests on self-centering concrete pier with external
581 dissipators and enhanced durability[J]. Journal of Structural Engineering, 2015, 142(1):
582 04015088.
583 [13] Han Q, Jia Z, Xu K, et al. Hysteretic behavior investigation of self-centering double-column
584 rocking piers for seismic resilience[J]. Engineering Structures, 2019, 188(1): 218-232.
585 [14] Tong T, Zhuo W, Jiang X, et al. Research on seismic resilience of prestressed precast segmental
586 bridge piers reinforced with high-strength bars through experimental testing and numerical
587 modelling[J]. Engineering Structures, 2019, 197:10335.
588 [15] Cai Z K, Wang D, Wang Z. Full-scale seismic testing of concrete building columns reinforced

589 with both steel and CFRP bars[J]. Composite Structures, 2017, 178: 195-209.
590 [16] Roh H, Reinhorn A M. Hysteretic behavior of precast segmental bridge piers with superelastic
591 shape memory alloy bars[J]. Engineering Structures, 2010, 32(10): 3394-3403.
592 [17] Japan Road Association. specifications for highway bridges-Part V Seismic design[M]. Tokyo:
593 Marusan Publishing, 2002.
594 [18] Liossatou E, Fardis M N. Near-fault effects on residual drifts of RC structures[J]. Earthquake
595 Engineering & Structural Dynamics, 2016, 45(9):1391-1409.
596 [19] Cheng H, Li H, Wang D, et al. Research on the influencing factors for residual drifts of RC
597 bridge columns subjected to earthquake loading[J]. Bulletin of Earthquake Engineering, 2016,
598 14(8):2229-2257.
599 [20] Liossatou E, Fardis M N. Residual drifts of RC structures as SDOF systems[J]. Earthquake
600 Engineering & Structural Dynamics, 2015, 44(5):713-734.
601 [21] Ji D, Wen W, Zhai C, et al. Residual drift ratios of SDOF systems subjected to ground motions
602 recorded on soft soils[J]. Soil Dynamics & Earthquake Engineering, 2018, 115:331-335.
603 [22] Amiri S, Bojorquez E. Residual drift ratios of structures under mainshock-aftershock
604 sequences[J]. Soil Dynamics & Earthquake Engineering, 2019, 121:179-193.
605 [23] Zhan S, Jian Z. Dimensional estimation of residual-drift demands for bilinear bridges under
606 near-fault ground motions[J]. Journal of Bridge Engineering, 2018, 23(11):04018087.
607 [24] Quinde P, Teran A, Reinoso E. Residual drift estimation for soft soils: Application to Mexico
608 city lake-bed[J]. Soil Dynamics & Earthquake Engineering, 2019, 130:105970.
609 [25] Li S, Zhao T, Alam MS, et al. Probabilistic seismic vulnerability and loss assessment of a
610 seismic resistance bridge system with post-tensioning precast segmental ultra-high performance
611 concrete bridge columns[J]. Engineering Structures, 2020, 225: 111321.
612 [26] Ou Y C, Chiewanichakorn M, Aref A J, et al. Seismic performance of segmental precast
613 unbonded posttensioned concrete bridge columns[J]. Journal of Structural Engineering, 2007,
614 133(11):1636-1647.
615 [27] Cai Z, Zhou Z, Wang Z. Influencing factors of residual drifts of precast segmental bridge
616 columns with energy dissipation bars[J]. Advances in Structural Engineering, 2019,
617 22(1):126-140.
618 [28] Liu X, Li J, Tsang H H, et al. Evaluating self-centering behavior of unbonded prestressed bridge

columns using a new performance index based on quasi-static analysis[J]. Journal of Earthquake & Tsunami, 2018, 12:1850001.

[29] Wang Z, Wang J, Zhao G, et al. Design criterion for the self-centering capacity of precast segmental UHPC bridge columns with unbonded post-tensioning tendons[J]. Engineering Structures, 2019, 200: 109706.

[30] Ahmdi E, Kashani M M. Numerical investigation of nonlinear static and dynamic behaviour of self-centring rocking segmental bridge piers[J]. Soil Dynamics & Earthquake Engineering, 2020, 128: 105876.

[31] Marriott D, Pampanin S, Palermo A. Quasi-static and pseudo-dynamic testing of unbonded post-tensioned rocking bridge piers with external replaceable dissipaters[J]. Earthquake Engineering & Structural Dynamics, 2009, 38(3): 331-354.

[32] Priestley M J N, Calvi G M, Kowalsky M J. Displacement-based seismic design of structures[M]. Pavia: IUSS Press, 2007.

[33] Kowalsky M J, Priestley M J N, Macrae G A. Displacement-based design of RC bridge columns in seismic regions[J]. Earthquake Engineering & Structural Dynamics, 1995, 24(12): 1623-1643.

[34] Mantawy I M, Sanders D H, Eberhard M O, et al. Modelling of debonded reinforcement in ABC connections designed for seismic zones[J]. Engineering Structures, 2019, 198: 109351.

[35] Pampanin S, Priestley M J N, Sritharan S. Analytical modelling of the seismic behaviour of precast concrete frames designed with ductile connections[J]. Journal of Earthquake Engineering, 2001, 5(03): 329-367.

[36] Bu Z Y, Ou Y C . Simplified Analytical Pushover Method for Precast Segmental Concrete Bridge Columns[J]. Advances in Structural Engineering, 2013, 16(5):805-822.

[37] Guo J, Xin K G, He M H, et al. Experimental study and analysis on the seismic performance of a self-centering bridge pier[J]. Engineering Mechanics, 2012(A01):29-34.

[38] Hieber, D.G, Wacker, J.M, et al. Precast concrete pier systems for rapid construction of bridges in seismic regions(No. WA-RD 611.1)[R]. University of Washington, Seattle, Washington, USA, 2005.

[39] Weng Y K, Pampanin S, Palermo A, et al. Self-centering structural systems with combination of hysteretic and viscous energy dissipations[J]. Earthquake Engineering & Structural Dynamics, 2010, 39(10).

649 [40] Pampanin S, Priestley M J N, Sritharan S. Analytical modelling of the seismic behaviour of
650 precast concrete frames designed with ductile connections[J]. Journal of Earthquake Engineering,
651 2001, 5(03): 329-367.
652 [41] Montgomery D C. Design and analysis of experiments[M]. New York: John Wiley and Sons,
653 2008.